nature communications

Article

https://doi.org/10.1038/s41467-024-45671-8

Low-frequency vibrational density of states of ordinary and ultra-stable glasses

Received: 23 August 2023

Accepted: 1 February 2024

Published online: 16 February 2024

Check for updates

Ding Xu[1,2,4], Shiyun Zhang[1,2,4], Hua Tong[2], Lijin Wang[3] ✉ & Ning Xu[1,2] ✉

A remarkable feature of disordered solids distinct from crystals is the violation of the Debye scaling law of the low-frequency vibrational density of states. Because the low-frequency vibration is responsible for many properties of solids, it is crucial to elucidate it for disordered solids. Numerous recent studies have suggested power-law scalings of the low-frequency vibrational density of states, but the scaling exponent is currently under intensive debate. Here, by classifying disordered solids into stable and unstable ones, we find two distinct and robust scaling exponents for non-phononic modes at low frequencies. Using the competition of these two scalings, we clarify the variation of the scaling exponent and hence reconcile the debate. Via the study of both ordinary and ultra-stable glasses, our work reveals a comprehensive picture of the low-frequency vibration of disordered solids and sheds light on the low-frequency vibrational features of ultra-stable glasses on approaching the ideal glass.

Low-temperature properties of solids, such as specific heat and thermal conductivity, are closely related to the excitation of low-frequency vibrational states. For crystals, it is well-established that the vibrational states, i.e., phonons, form a low-frequency vibrational density of states (VDOS) following the Debye scaling law: $D(\omega) \sim \omega^{d-1}$, where ω is the frequency and d is the spatial dimension, resulting in the T^d scaling of the specific heat at low temperatures T[1]. The thermal conductivity is believed to be governed by the specific heat, phonon mean free path, and sound velocity. In crystals, because the phonon mean free path and sound velocity remain approximately constant in temperature, the thermal conductivity follows the low-temperature scaling of the specific heat[1].

However, we face great challenges when dealing with disordered solids such as glasses. The low-temperature scalings of the specific heat and thermal conductivity are no longer T^{d}[2–4]. When $T < 1K$, the specific heat is linearly scaled with T[2–4], which is attributed largely to the existence of two-level systems instead of the VDOS[5,6]. It is also believed that the two-level systems change the mean free path, causing anomalous behaviors of the thermal conductivity. At higher temperatures, the VDOS matters. The disordered structure of glasses causes the coexistence of phonon-like and non-phononic modes at low frequencies[7–14], so the VDOS is at least a superposition of the Debye scaling and that of the non-phononic modes. The excess non-phononic modes form a peak in $D(\omega)/\omega^{d-1}$, defined as the boson peak[11,12,15]. It has been shown that the boson peak may be correlated with the simultaneity of the peak in c_p/T^3, with c_p being the constant-pressure specific heat, and the plateau in the thermal conductivity at the boson peak temperature (~$10K$ for typical glasses such as vitreous silica)[4]. Both simulations and experimental measurements such as the neutron scattering and X-ray, have significantly advanced our understanding of the constituent modes of the boson peak[11–16]. However, what the VDOS of non-phononic modes looks like below the boson peak frequency is still an unsettled issue[7,8,17–31], which is crucial to understanding the thermal properties in the 1–$10K$ temperature regime. In addition to the thermal properties, the anomalous low-frequency non-phononic modes have been successfully applied to understand various other properties of disordered solids, e.g., mechanical failure[32–37], glass transition[13,38,39], and heterogeneous dynamics of glass-forming liquids[40–42].

[1]Hefei National Research Center for Physical Sciences at the Microscale and CAS Key Laboratory of Microscale Magnetic Resonance, University of Science and Technology of China, Hefei 230026, P. R. China. [2]Department of Physics, University of Science and Technology of China, Hefei 230026, P. R. China. [3]School of Physics and Optoelectronic Engineering, Information Materials and Intelligent Sensing Laboratory of Anhui Province, Anhui University, Hefei 230601, P. R. China. [4]These authors contributed equally: Ding Xu and Shiyun Zhang. ✉e-mail: lijin.wang@ahu.edu.cn; ningxu@ustc.edu.cn

Numerous recent studies suggest that the low-frequency VDOS of non-phononic modes exhibits the ω^{α} scaling with $\alpha \neq d-1$[7,8,17–31]. However, the value of the exponent α is still under debate. A popular argument is that $\alpha = 4$ for generic glasses[7,8,17–19], i.e., zero-temperature disordered solids, which are constrained well above isostaticity and are thus not governed by the jamming physics[43,44]. It has been claimed that the quartic scaling is independent of spatial dimensions[18,21] and interaction potentials[19] and is valid for low-temperature glasses as well[45]. There are theories supporting this scaling, e.g., mean-field theories based on replica[46,47] and effective medium approximation[48,49], and phenomenological theories[50–53]. However, some other studies also reported deviations of α from 4. It has been shown that α may vary with the glass stability[22,23], system size[20,21,24], stress distribution[25], and frequency range accessed[26–29]. There are also models arguing that $\alpha \neq 4$. For example, the fluctuating elasticity theory predicts $\alpha = d+1$[54,55]; the fold instability argument predicts $\alpha \approx 3$[36], independent of spatial dimensions.

Note that generic glasses lie at local minima of the complex energy landscape[56], whose stabilities can vary a lot from each other. One can tell that the variation of α mentioned above is more or less related to the stability. However, the local minima with various degrees of stability were always mixed up to calculate the VDOS in previous studies. Moreover, probably limited by the development of experimental techniques, as far as we know, there have been no direct experimental measurements of α for molecular glasses. Therefore, the examination of α has heavily relied on simulations. In most of previous simulations, the VDOS was calculated for systems with periodic boundary conditions, whose shapes were not allowed to change. However, it has been shown that some glasses that are stable under periodic boundary conditions may be unstable under certain deformations[57,58]. Apparently, the effects of such deformation stability on the VDOS were completely overlooked.

Here, we systematically study the low-frequency VDOS for both ordinary and ultra-stable model glasses quenched from different parent temperatures T_p. Remarkably different from previous approaches, we divide all glasses into two categories: stable ones, which can resist any infinitesimal deformations, and unstable ones, which are unstable subject to some infinitesimal deformations, and calculate their VDOSs separately. The VDOSs for stable and unstable solids depart from each other below a crossover frequency ω_d, where they have different scaling exponents. For unstable solids, $\alpha = \alpha_u \approx 3.3$, independent of system size and spatial dimension. For stable solids, $\alpha = \alpha_s \approx 5.5$ and 6.5 in 2D ($d = 2$) and 3D ($d = 3$), respectively, which does not vary with system size either. The superposition of these two VDOSs results in the VDOS studied in previous approaches. This explains the variation of α under various circumstances. Moreover, we observe the emergence of an ω^4 scaling right above the ω^{α_s} one when the system size of stable solids increases for both ordinary and ultra-stable glasses in 3D. Interestingly, our results suggest that the number of non-phononic modes forming the ω^{α_s} and ω^4 scalings decays with the decrease of T_p, possibly vanishing at a sufficiently low T_p. Therefore, our study may shed light on the perspective of the vibrational features of the ideal glass.

Results

In this work, we mainly show results for systems composed of polydisperse soft particles interacting via the inverse-power-law (IPL) potential (see Methods for details), which have been widely used to study the glass transition[8,26,28,59–62]. In Supplementary Fig. 1 of the Supplementary Information and a parallel study, we also show consistent results for Lennard–Jones and harmonic potentials, suggesting the generality of our findings. We obtain the zero-temperature glasses by instantaneously quenching liquids equilibrated at the parent temperature T_p. It is well-known that the stability of quenched glasses increases with the decrease of T_p when T_p is lower than the onset temperature T_{on}, i.e., the crossover temperature from Arrhenius to super-Arrhenius dynamics[56]. We will first study glasses obtained from a given T_p and discuss the T_p dependence afterward.

VDOSs for stable and unstable solids

In most of the previous simulations, the normal modes of vibration were obtained from the diagonalization of the normal Hessian matrix, with the elements being the second derivatives of the potential energy with respect to particle coordinates. No boundary deformation was taken into account in such an approach. A glass was treated as a stable one if all nontrivial eigenvalues of the normal Hessian matrix were positive. However, this cannot guarantee that the glass is stable subject to boundary deformations. If we introduce the $d(d+1)/2$ degrees of freedom corresponding to the boundary deformations (shear and compression) and construct the extended Hessian matrix (see Methods), the matrix of some glasses may have negative eigenvalues, indicating that the glasses are unstable under some deformations. We thus define these glasses as unstable glasses. On the other hand, the glasses whose extended Hessian matrix has no negative eigenvalues are defined as stable glasses. Note that the extended Hessian matrix is only used to classify all glasses into stable and unstable ones, and VDOS is still calculated from the normal Hessian matrix. Here, we denote $D_s(\omega)$, $D_u(\omega)$, and $D(\omega)$ as the VDOSs of stable, unstable, and all glasses, respectively.

Figure 1a, b compares $D(\omega)$, $D_s(\omega)$, and $D_u(\omega)$ in 2D and 3D, respectively. They collapse above a crossover frequency ω_d, and depart from each other otherwise. Both low-frequency tails of $D_s(\omega)$ and $D_u(\omega)$ display a clear power-law scaling behavior, $D_s(\omega) \sim \omega^{\alpha_s}$ and $D_u(\omega) \sim \omega^{\alpha_u}$. Beyond that, $D_u(\omega)$ forms a valley bottomed at ω_d, while $D_s(\omega)$ still monotonically increases and transits to ω_d. However, α_s and α_u are apparently different. In 2D and 3D, $\alpha_s = 5.5 \pm 0.2$ and 6.5 ± 0.2, respectively. In contrast, $\alpha_u = 3.3 \pm 0.1$ in both 2D and 3D. This α_u value is close to the $\alpha \approx 3$ arguments of the fold instability model[36]. Note that $\alpha \approx 3$ is obtained based on the approximation that the distribution of the stress distance to instabilities is constant[36], which may fluctuate if the distribution is not strictly flat. The fold instability model is raised

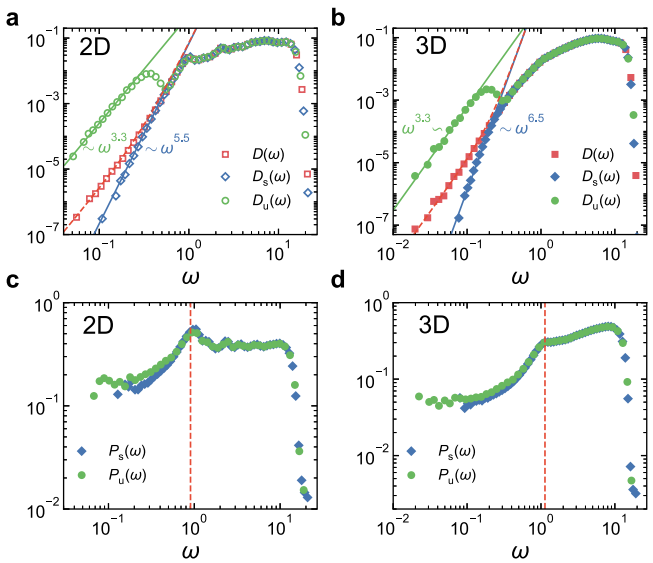

Fig. 1 | Comparison of VDOS and participation ratio of stable, unstable, and all glasses. a VDOSs of 2D systems with $N = 256$ and $T_p = 0.12$. **b** VDOSs of 3D systems with $N = 1000$ and $T_p = 0.18$. The solid lines are power-law fittings to $D_s(\omega)$ and $D_u(\omega)$ at low frequencies. The red dashed lines are results from Eq. (1). They are in excellent agreement with the simulated $D(\omega)$ at low frequencies. **c** and **d** show the participation ratio of stable and unstable solids for the same systems in (**a**) and (**b**), respectively. The vertical dashed lines mark the frequency of the first Goldstone mode.

for glasses with weak stability and is prone to rearrangement upon deformations and does not rely on spatial dimension. This agreement thus proposes a plausible physical origin of the scaling behavior of $D_u(\omega)$.

By definition, the low-frequency part of $D(\omega)$ should be the superposition of $D_s(\omega)$ and $D_u(\omega)$:

$$\begin{aligned} D(\omega) &= f_s D_s(\omega) + (1-f_s) D_u(\omega) \\ &= f_s A_s \omega^{\alpha_s} + (1-f_s) A_u \omega^{\alpha_u}, \end{aligned} \tag{1}$$

where f_s is the fraction of stable glasses, and A_s and A_u are prefactors of $D_s(\omega)$ and $D_u(\omega)$, respectively. In Fig. 1a, b, we compare the simulated $D(\omega)$ with the prediction by Eq. (1) (dashed line). They are in excellent agreement at low frequencies.

As done in previous studies, the low-frequency part of $D(\omega)$ can be fitted with ω^{α}. Figure 1a, b indicates that α should be between α_u and α_s, if we perform the fitting. Now, the excellent agreement between $D(\omega)$ and Eq. (1) provides another interpretation of the α value at the low-frequency tail. If the values of α_s and α_u are definite, the α value is jointly determined by f_s, A_s, and A_u, which may change with parameters such as system size and parent temperature. We are thus able to understand why α was reported to vary under some circumstances[20–24]. Moreover, at low enough frequencies, $D_u(\omega)$ dominates. This may be the reason why lower values of α were always observed when rather low-frequency regimes were accessed[24,27,28].

Figure 1c, d compares the participation ratio, $P_s(\omega)$ and $P_u(\omega)$, of stable and unstable solids. A mode with a lower participation ratio is more localized. We can see that, below the first Goldstone (phonon-like) mode, the low-frequency modes forming the ω^{α_s} and ω^{α_u} scalings have the lowest participation ratios and are thus most quasi-localized on average. However, the degrees of quasi-localization of stable and unstable solids are similar, only that unstable solids extend to lower frequencies.

Figure 2a, b visualizes the structures of the modes lying in the ω^{α_u} and ω^{α_s} scaling regimes. They both exhibit the typical feature of quasi-localized modes with localized regions hybridizing with the plane-wave-like background. For the unstable solid in Fig. 2a, we show in Fig. 2c its unstable mode of the extended Hessian matrix, whose eigenvalue is negative. It looks almost identical to the mode in Fig. 2a. The dot product of the two normalized modes in Fig. 2a, c is 0.997. Note that when a disordered solid approaches the fold instability under load such as shear and compression, its lowest-frequency mode is responsible for the instability, whose frequency decays to zero following a power law while its structure remains unchanged[36]. This type of mode contributes to the ω^3 behavior predicted by the fold instability argument[36]. Therefore, the perfect agreement between the lowest-frequency mode of the unstable solid and the unstable mode of the extended Hessian matrix is the evidence supporting our argument that $\alpha_u \approx 3.3$ originates from fold instabilities. Figure 2d illustrates how the boundary deforms associated with the unstable mode of the extended Hessian matrix shown in Fig. 2c. It involves both shear and

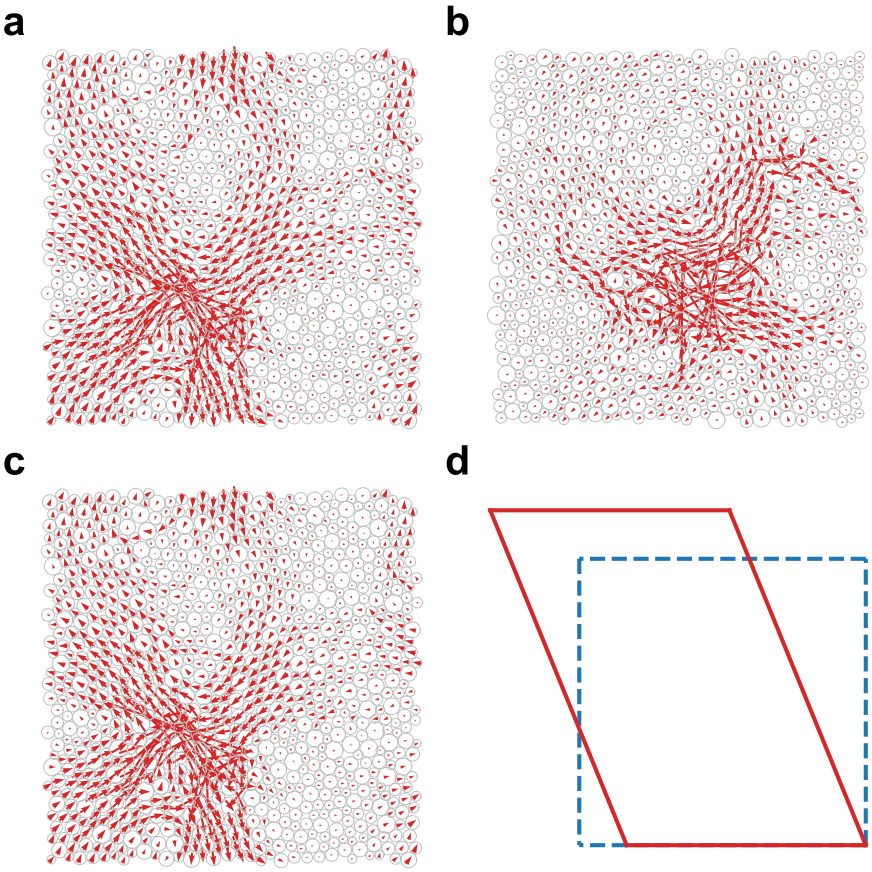

Fig. 2 | Visualization of the lowest-frequency modes of stable and unstable solids. a Structure of the lowest-frequency mode of an unstable solid. **b** Structure of the lowest-frequency mode of a stable solid. Here, we show 2D examples with $N = 1024$ and $T_p = 0.25$. The red arrows show the polarization vectors of particles. The modes lie in the ω^{α_u} and ω^{α_s} regimes, respectively. **c** Structure of the unstable mode with the lowest and negative eigenvalue of the extended Hessian matrix for the same unstable solid in (**a**). It looks almost identical to that in (**a**). The dot production of the normalized polarization vectors in (**a**) and (**c**) is 0.997. **d** Illustration of the boundary deformation associated with the unstable mode in (**c**). The ratio of three strains (see Methods) is $\epsilon_{xx} : \epsilon_{yy} : \epsilon_{xy} = -0.359 : 0.352 : -1$. The deformation involves both shear and compression (expansion).

compression, which is the typical form of the boundary deformation of unstable modes.

System size dependence

Recently, it was reported that the value of α for $D(\omega)$ increased with the growth of system size for ordinary glasses quenched from high parent temperatures[20,21,24]. As shown in Fig. 3a, for 2D systems, α indeed grows from 3.4 to 4 when the system size N changes from 256 to 4096. Interestingly, Fig. 3b, c shows that α_s and α_u remain constant in N. However, both A_s and A_u grow with N. Meanwhile, f_s increases when N increases, which can be fitted well with $1-f_s \sim N^{-1.4}$, as illustrated in Fig. 3d. Therefore, the system size dependence of α in 2D directly reflects the competition among f_s, A_s, and A_u.

Figure 3 e–h indicates that similar system size evolution happens in 3D. When system size increases, α gradually increases. Again, α_s and α_u are insensitive to the change in system size, while A_s, A_u, and f_s grow with N. However, the comparison between Fig. 3b, f demonstrates a seeming difference between 2D and 3D. In 2D, the ω^{α_s} scaling extends all the way to the crossover frequency ω_d, above which $D_s(\omega)$ and $D_u(\omega)$ collapse. In 3D, the ω^{α_s} scaling is deviated above another crossover frequency $\omega_s < \omega_d$. Figure 3f shows that, when system size increases, ω_s decreases so that the frequency regime for the ω^{α_s} scaling to survive is suppressed.

In addition to ω_d and ω_s, there is another characteristic frequency $\omega_p < \omega_d$ of the first peak in $D_u(\omega)$. In Fig. 3d, h, we show the system size dependence of these three characteristic frequencies. In both 2D and 3D, ω_d is approximately scaled with $N^{-1/d}$. Since $D_s(\omega)$ and $D_u(\omega)$ deviate below ω_d, if such system size dependence persists on approaching the thermodynamic limit, we would expect that the ω^{α_s} and ω^{α_u} scalings tend to disappear so that $D_s(\omega)$ and $D_u(\omega)$ eventually become identical to $D(\omega)$. Note that the Goldstone modes have the same system size dependence. It may be plausible to ask whether ω_d is associated with some inherent properties of disordered solids such as the elastic moduli, which contribute to the Goldstone modes. Figure 3d, h shows that ω_p is approximately scaled with $N^{-0.55}$ in both 2D and 3D. As seen from Fig. 3h, $\omega_s(N)$ in 3D roughly agrees with $\omega_p(N)$. At the current stage, we are not able to confirm whether there are any physical origins of these characteristic frequencies and hope to leave them to future investigations.

In Fig. 4, we collapse the low-frequency parts of $D_s(\omega)$ and $D_u(\omega)$ for different system sizes by plotting $N^{-\nu_s}D_s(\omega)$ and $N^{-\nu_u}D_u(\omega)$ against ωN^{ν_s} and ωN^{ν_u}, respectively. These scalings conserve the integrals of the VDOSs. Our best data collapse gives $\nu_s \approx 0.21$ for both 2D and 3D and $\nu_u \approx 0.35$ and 0.28 for 2D and 3D, respectively. The scaling collapse indicates that $A_s \sim N^{(\alpha_s+1)\nu_s}$ and $A_u \sim N^{(\alpha_u+1)\nu_u}$, respectively.

Seen from Fig. 3f, the $\omega > \omega_s$ part of $D_s(\omega)$ in 3D shows the trend to converge to a master curve when system size increases. Figure 3f also indicates that $D_s(\omega)$ reaches the maximum at $\omega = \omega^* \approx 5$, above which $D_s(\omega)$ is plateau-like and gradually decreases. In Fig. 5a, we focus on $\omega < \omega^*$ with more system sizes. There seem to be three consecutive frequency regimes with different scalings: (i) ω^{α_s} when $\omega < \omega_s$, (ii) ω^{α_1} when $\omega_s < \omega < \omega_0$, and (iii) ω^{α_2} when $\omega_0 < \omega < \omega^*$. Unlike the size-independent α_s, α_1 and α_2 evolve with N. For the largest system sizes studied here, we can observe the emergence of $\alpha_1 \approx 4$ and $\alpha_2 \approx 1.5$. Right below the plateau of the VDOS ($\omega_0 < \omega < \omega^*$), mean-field theories predict an ω^2 behavior due to marginal stability[63,64]. For the system sizes studied here, α_2 slightly varies with system size. Although we are not able to exclude the possibility that α_2 could approach 2 in sufficiently large systems, $\alpha_2 \approx 1.5$ observed here is still apparently lower than the mean-field value. It thus remains a question whether α_2 is meaningful and related to marginal stability. Recent studies suggest that quasi-localized modes below ω_0 could form the ω^4 scaling. Here, we see this scaling right above ω_s. However, whether this scaling is real or is just a crossover still needs to be examined in sufficiently large systems with good statistics. Note that, even if ω^4 could be real, our results suggest that it does not generally exist. As shown in Fig. 3b, in 2D, there is no sign for the ω^4 behavior to emerge in $D_s(\omega)$.

Assuming that the system size evolution of ω_s is still valid in much larger systems, we can expect that there is always a contribution of the ω^{α_s} scaling below ω_s, as long as the system size is finite. Therefore, the low-frequency tail of $D(\omega)$ is always jointly determined by $D_s(\omega)$ and $D_u(\omega)$ according to Eq. (1).

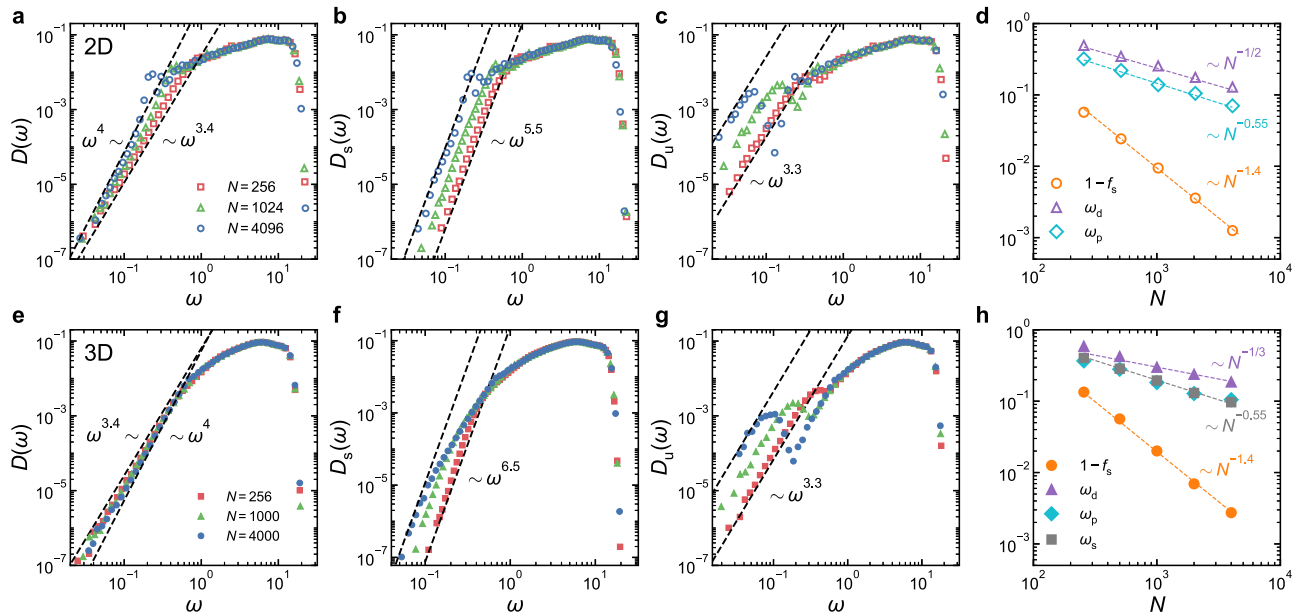

Fig. 3 | System size dependence of the VDOSs. a–d VDOSs of all stable and unstable glasses, $D(\omega)$, $D_s(\omega)$, and $D_u(\omega)$, in 2D and system size evolution of the fraction of stable glasses f_s, the frequency ω_p of the first peak in $D_u(\omega)$, and the frequency ω_d below which $D_u(\omega)$ and $D_s(\omega)$ depart from each other, respectively. **e–h** Results in 3D. In (**h**), we also show the system size depends of the frequency ω_s below which the ω^{α_s} scaling exists. The parent temperature T_p is approximately the onset temperature T_{on} for both 2D and 3D systems. The dashed lines show the power-law scalings.

https://doi.org/10.1038/s41467-024-45671-8

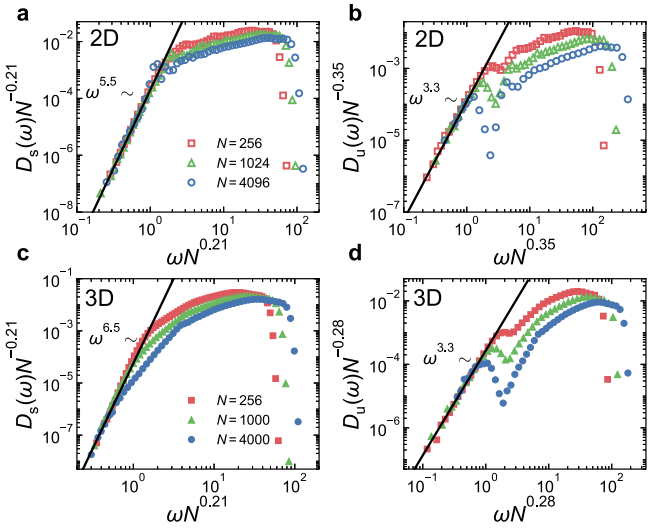

Fig. 4 | Scaling collapse of the low-frequency parts of the VDOSs for different system sizes. The VDOSs of stable and unstable glasses, $D_s(\omega)$ and $D_u(\omega)$, collapse at low frequencies, when $D_s(\omega)N^{-\nu_s}$ and $D_u(\omega)N^{-\nu_u}$ are plotted against ωN^{ν_s} and ωN^{ν_u}, respectively. Results of 2D glasses are shown in (**a**) and (**b**), while (**c**) and (**d**) show results of 3D glasses. Here $\nu_s = 0.21$ for both 2D and 3D; $\nu_u = 0.35$ and 0.28 for 2D and 3D, respectively. The solid lines are power-law fittings to the collapsed curves.

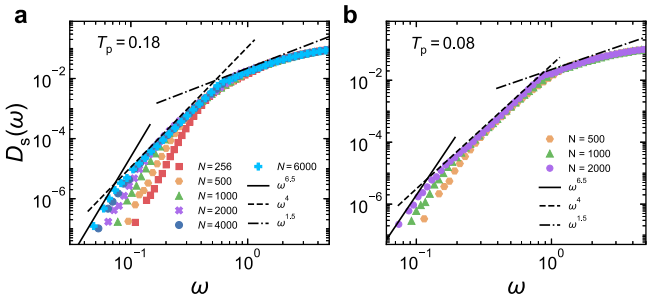

Fig. 5 | System size evolution of the VDOS of stable glasses in 3D. a $D_s(\omega)$ of ordinary glasses quenched from $T_p = 0.18$. **b** $D_s(\omega)$ of ultra-stable glasses quenched from $T_p = 0.08$. The solid, dashed, and dot-dashed lines show the ω^{α_s}, ω^4, and $\omega^{1.5}$ scalings, respectively.

Parent temperature dependence

It was also reported that α grew when the parent temperature T_p decreased[22,23]. To understand this T_p dependence, we study the VDOSs of glasses quenched from various T_p ranging from above the onset temperature T_{on} to near the glass transition temperature T_g. Figure 6 compares $D(\omega)$, $D_s(\omega)$, and $D_u(\omega)$ near the three representative temperatures, T_{on}, T_{mc} (mode-coupling temperature), and T_g, for both 2D and 3D glasses. Figure 6a, e shows that α evolves roughly from 3.4 to 4 when T_p decreases from T_{on} to T_g in both 2D and 3D, consistent with previous studies[22,24] and similar to the evolution with system size. The difference is that the low-frequency part of $D(\omega)$ apparently decays with the decrease of T_p. Figure 6b, c (f and g) indicates that α_s and α_u also remain constant in T_p in 2D (3D). Unlike the system size dependence, A_u is insensitive to the change of T_p. Therefore, the evolution of $D(\omega)$ at low frequencies is jointly determined by A_s and f_s. When T_p decreases, Fig. 6b, f shows that A_s decreases, while f_s increases, as shown in Fig. 6d, h.

For 3D ultra-stable glasses quenched from $T_p \approx T_g$, Fig. 5b shows that the three frequency regimes in $D_s(\omega)$ discussed above also emerge. Compared to the high T_p case, the intermediate ω^4 scaling seems to be more pronounced. For example, for smaller systems with $N \le 1000$, there is no apparent ω^4 scaling in Fig. 5a, but we can already see it in Fig. 5b. Again, the authenticity of the ω^4 scaling needs to be verified in sufficiently large systems, which is however still absent in 2D ultra-stable glasses.

Figure 7 directly displays the T_p dependence of A_s. For 3D systems, we also show the prefactor A_4 of the ω^4 scaling above ω_s. Both A_s and A_4 keep decreasing with the decrease of T_p. Similar T_p dependence was reported for the prefactor of the ω^4 scaling of $D(\omega)$[8,31]. At the current stage, it is difficult to obtain reliable results at much lower T_p. If such T_p dependence persists at even lower T_p, the number of low-frequency non-phononic modes significantly decreases and could be expected to vanish at low enough T_p. If this is the case, such low-temperature ultra-stable glasses will only have phonon-like modes at low frequencies. Although structurally disordered, evaluated by conventional criteria, the glasses could behave like crystals at long wavelengths. In fact, there was experimental evidence of the low-temperature Debye scaling for ultra-stable glasses[65–67], supporting that the non-phononic mode contribution can be negligible if the glass reaches the highest stability. It is thus interesting to figure out whether such ultra-stable glasses are prototypes of ideal glasses and under what temperatures they could exist.

Discussion

By classifying disordered solids into stable and unstable ones, we find that their VDOSs, $D_s(\omega)$ and $D_u(\omega)$, depart from each other when $\omega < \omega_d$, with the low-frequency tails following distinct scaling laws, $D_s(\omega) \sim \omega^{\alpha_s}$ and $D_u(\omega) \sim \omega^{\alpha_u}$, respectively. The robustness of the values of α_s and α_u is verified by the solids with different sizes and quenched from different parent temperatures. Using this classification, we can understand the variation of the scaling exponent α reported previously. For finite-size disordered solids, it is due to the existence of unstable solids and the competition among the fraction of (un)stable solids and prefactors of the two scalings. Because unstable solids are inevitable in confined systems, our study can explain a recent experimental observation of $\alpha \approx 3$ in a confined quasi-2D nanosystem[68].

We also find that when system size increases, ω_d decreases so that the two scalings are pushed to lower frequencies. For stable solids in 3D, the ω^{α_s} scaling only exists below another crossover frequency $\omega_s < \omega_d$, which also decreases with the increase of system size. When $\omega > \omega_s$, our results show the trend of the emergence of the ω^4 scaling in the largest systems studied and ultra-stable glasses. At the current stage, we cannot confirm the authenticity of the ω^4 scaling, which requires the verification of sufficiently large systems in future studies. For stable solids in 2D, we do not see the emergence of the ω^4 scaling. Moreover, the prefactors of the ω^{α_s} and ω^4 scalings both decrease with the decrease of parent temperature, implying the possible existence of ultra-stable glasses with only crystal-like low-frequency vibrations at low enough temperatures. Such glasses may act as prototypes of the ideal glass.

In this work, we are focused on generic glasses, which are constrained well above isostaticity[43,44,69,70]. Marginally jammed solids near isostaticity are less stable than generic glasses concerned here. It is thus interesting to know whether and to what extent our findings here are applicable to marginally jammed solids. There are mean-field theories proposing the $\alpha = 2$ scaling of the VDOS[63,64]. The competition between different theoretical frameworks may complicate the vibrational features of marginally jammed solids moving away from the jamming transition[43,44]. We leave these discussions to a separate study.

Methods

Simulation model

Our systems contain N polydisperse particles in a simulation cell with side length L and periodic boundary conditions in all directions. All particles have the same mass m. Particles i and j interact via the IPL

https://doi.org/10.1038/s41467-024-45671-8

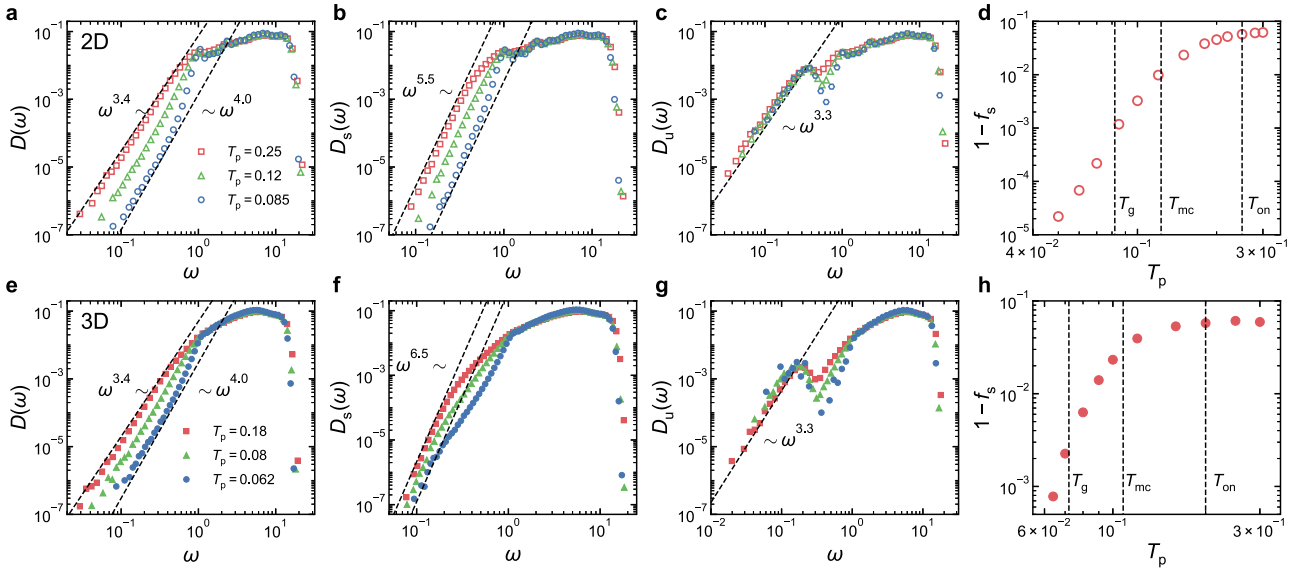

Fig. 6 | Parent temperature dependence of the VDOSs. a–d VDOSs of all stable, and unstable glasses, $D(\omega)$, $D_s(\omega)$, and $D_u(\omega)$, and parent temperature evolution of the fraction of stable glasses f_s for $N = 256$ systems in 2D. **e–h** Results for $N = 1000$ systems in 3D. The vertical dashed lines in (**d**) and (**h**) locate T_{on}, T_{mc}, and T_g, respectively. The dashed lines in the other panels show the power-law scalings.

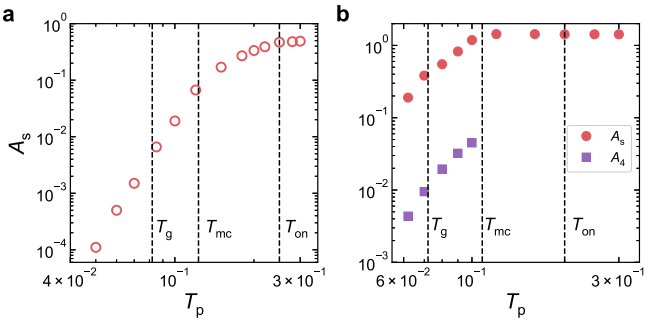

Fig. 7 | Parent temperature dependence of prefactors of the VDOS of stable glasses. a Prefactor A_s versus T_p in 2D. **b** Prefactors A_s and A_4 versus T_p in 3D. The vertical dashed lines locate T_{on}, T_{mc}, and T_g, respectively.

potential:

$$U(r_{ij}) = \left(\frac{\sigma_{ij}}{r_{ij}}\right)^{12} + c_0 + c_2\left(\frac{r_{ij}}{\sigma_{ij}}\right)^2 + c_4\left(\frac{r_{ij}}{\sigma_{ij}}\right)^4, \tag{2}$$

when their separation $r_{ij} \le 1.25\sigma_{ij}$, and zero otherwise. The coefficients c_0, c_2, and c_4 ensure the continuity of the potential up to the second derivative at the cutoff. The particle diameter σ is extracted from a continuous distribution $P(\sigma) = A\sigma^{-3}$, where A is the normalization factor and $\sigma \in [\sigma_m, \sigma_M]$ with $\sigma_m/\sigma_M = 0.4492$. To enhance the glass-forming ability, we adopt a non-additive mixing rule to determine σ_{ij} in Eq. (2):

$$\sigma_{ij} = \frac{\sigma_i + \sigma_j}{2}\left(1 - \epsilon|\sigma_i - \sigma_j|\right), \tag{3}$$

where ϵ measures the degree of non-additivity. We choose $\epsilon = 0.2$ to achieve a better performance[59].

We set the average particle diameter $\bar{\sigma}$, particle mass m, and the Boltzmann constant k_B to be 1. The number density $\rho = N/L^d$ is 1.01 and 1.0 for 2D and 3D, respectively.

We use an efficient swap Monte Carlo algorithm[59] to prepare well-equilibrated liquids at parent temperatures T_p. The onset, mode-coupling, and glass transition temperatures for our IPL model systems are $T_{on} \approx 0.25(0.20)$, $T_{mc} \approx 0.123(0.108)$, and $T_g \approx 0.082(0.072)$ in 2D (3D), respectively[8,60]. After equilibration at the parent temperature T_p, the liquids are rapidly quenched to zero temperature to obtain the zero-temperature glasses (inherent structures) via the fast inertial relaxation engine algorithm[71].

Vibrational quantities

We consider two types of Hessian matrix. The normal Hessian matrix is defined as

$$M_n = \frac{\partial^2 U}{\partial \mathbf{R}^2}, \tag{4}$$

where $\mathbf{R} = (\mathbf{r}_1, \mathbf{r}_2, \ldots, \mathbf{r}_N)$ with $\mathbf{r}_i$ $(i = 1, 2, \ldots, N)$ being the location of particle i. The normal Hessian matrix does not take any boundary deformation into account. In comparison, the extended Hessian matrix with $(dN + n_{ex}) \times (dN + n_{ex})$ dimensions is[58]

$$M_e = \frac{\partial^2 U}{\partial \tilde{\mathbf{R}}^2}, \tag{5}$$

where $n_{ex} = d(d+1)/2$ is the extra degrees of freedom of the system and $\tilde{\mathbf{R}} = (\mathbf{r}_1, \mathbf{r}_2, \ldots, \mathbf{r}_N, \epsilon_1, \epsilon_2, \ldots, \epsilon_{n_{ex}})$ with $\epsilon_i (i = 1, 2, \ldots, n_{ex})$ being the strain of the $i-$th deformation. The strains ϵ_i are upper triangular elements of the $d \times d$ strain tensor

$$\begin{pmatrix} \epsilon_{\beta_1\beta_1} & \epsilon_{\beta_1\beta_2} & \cdots & \epsilon_{\beta_1\beta_d} \\ \epsilon_{\beta_2\beta_1} & \epsilon_{\beta_2\beta_2} & \cdots & \epsilon_{\beta_2\beta_d} \\ \vdots & \vdots & \ddots & \vdots \\ \epsilon_{\beta_d\beta_1} & \epsilon_{\beta_d\beta_2} & \cdots & \epsilon_{\beta_d\beta_d}, \end{pmatrix} \tag{6}$$

where β_j $(j = 1, 2, \ldots, d)$ denotes the Cartesian coordinates. These n_{ex} degrees of freedom involve boundary deformations, including compression (expansion) and shear. More details and the stability analysis using the extended Hessian matrix can be found in Ref. 58. The normal modes of vibration are obtained by diagonalizing the matrix using the Intel Math Kernel Library[72]. If the extended Hessian matrix has negative eigenvalues, the system is unstable to certain boundary

deformations[58]. Otherwise, the system is stable to compression and shear in arbitrary directions. The participation ratio of a normal mode j is calculated as

$$P_j = \frac{\left(\sum_{i=1}^{N} |\mathbf{e}_i^j|^2\right)^2}{N \sum_{i=1}^{N} |\mathbf{e}_i^j|^4}, \quad (7)$$

where $\mathbf{e}_i^j$ is the polarization vector of particle i in mode j. In the calculation of the VDOSs and the participation ratio, we exclude some lowest-frequency localized modes caused by rattler-like particles, as explained in Supplementary Fig. 2 of the Supplementary Information.

Data availability

The data that support the findings of this study are included in the article and/or the Supporting Information and are available from the corresponding authors upon request.

Code availability

The computer codes of this study are available from the corresponding authors upon request.

References

1. Ashcroft, N. W. & Mermin, N. D. *Solid State Physics* (Thomson Learning, Toronto, 1976).
2. Zeller, R. C. & Pohl, R. O. Thermal conductivity and specific heat of noncrystalline solids. *Phys. Rev. B* **4**, 2029 (1971).
3. Pohl, R. O., Liu, X. & Thompson, E. Low-temperature thermal conductivity and acoustic attenuation in amorphous solids. *Rev. Mod. Phys.* **74**, 991 (2002).
4. Ramos, M. A. *Low-Temperature Thermal and Vibrational Properties of Disordered Solids* (World Scientific, 2022).
5. Phillips, W. A. Tunneling states in amorphous solids. *J. Low Temp. Phys.* **7**, 351–360 (1972).
6. Anderson, P. W., Halperin, B. I. & Varma, C. M. Anomalous low-temperature thermal properties of glasses and spin glasses. *Philos. Mag.* **25**, 1 (1972).
7. Mizuno, H., Shiba, H. & Ikeda, A. Continuum limit of the vibrational properties of amorphous solids. *Proc. Natl. Acad. Sci. USA* **114**, E9767–E9774 (2017).
8. Wang, L. et al. Low-frequency vibrational modes of stable glasses. *Nat. Commun.* **10**, 26 (2019).
9. Buchenau, U., Nücker, N. & Dianoux, A. J. Neutron scattering study of the low-frequency vibrations in vitreous silica. *Phys. Rev. Lett.* **53**, 2316 (1984).
10. Frick, B. & Richter, D. The microscopic basis of the glass transition in polymers from neutron scattering studies. *Science* **267**, 5206 (1995).
11. Ruocco, G. & Sette, F. High-frequency vibrational dynamics in glasses. *J. Phys.* **13**, 9141 (2001).
12. Nakayama, T. Boson peak and terahertz frequency dynamics of vitreous silica. *Rep. Prog. Phys.* **65**, 1195 (2002).
13. Xu, N., Wyart, M., Liu, A. J. & Nagel, S. R. Excess vibrational modes and the boson peak in model glasses. *Phys. Rev. Lett.* **98**, 175502 (2007).
14. Shintani, H. & Tanaka, H. Universal link between the boson peak and transverse phonons in glass. *Nat. Mater.* **7**, 870 (2008).
15. Grigera, T. S., Martin-Mayor, V., Parisi, G. & Verrocchio, P. Phonon interpretation of the boson peak in supercooled liquids. *Nature* **422**, 289–292 (2003).
16. Mahajan, S. & Ciamarra, M. P. Unifying description of the vibrational anomalies of amorphous materials. *Phys. Rev. Lett.* **127**, 215504 (2021).
17. Lerner, E., Düring, G. & Bouchbinder, E. Statistics and properties of low-frequency vibrational modes in structural glasses. *Phys. Rev. Lett.* **117**, 035501 (2016).
18. Kapteijns, G., Bouchbinder, E. & Lerner, E. Universal nonphononic density of states in 2D, 3D, and 4D glasses. *Phys. Rev. Lett.* **121**, 055501 (2018).
19. Richard, D. et al. Universality of the nonphononic vibrational spectrum across different classes of computer glasses. *Phys. Rev. Lett.* **125**, 085502 (2020).
20. Lerner, E. Finite-size effects in the nonphononic density of states in computer glasses. *Phys. Rev. E* **101**, 032120 (2020).
21. Das, P., Hentschel, H. G. E., Lerner, E. & Procaccia, I. Robustness of density of low-frequency states in amorphous solids. *Phys. Rev. B* **102**, 014202 (2020).
22. Lerner, E. & Bouchbinder, E. Effect of instantaneous and continuous quenches on the density of vibrational modes in model glasses. *Phys. Rev. E* **96**, 020104(R) (2017).
23. Paoluzzi, M., Angelani, L., Parisi, G. & Ruocco, G. Relation between heterogeneous frozen regions in supercooled liquids and non-Debye spectrum in the corresponding glasses. *Phys. Rev. Lett.* **123**, 155502 (2019).
24. Lerner, E. & Bouchbinder, E. Nonphononic spectrum of two-dimensional structural glasses. *J. Chem. Phys.* **157**, 166101 (2022).
25. Krishnan, V. V., Ramola, K. & Karmakar, S. Universal non-Debye low-frequency vibrations in sheared amorphous solids. *Soft Matter* **18**, 3395–3402 (2022).
26. Wang, L., Szamel, G. & Flenner, E. Low-frequency excess vibrational modes in two-dimensional glasses. *Phys. Rev. Lett.* **127**, 248001 (2021).
27. Wang, L., Fu, L. & Nie, Y. Density of states below the first sound mode in 3D glasses. *J. Chem. Phys.* **157**, 074502 (2022).
28. Wang, L., Szamel, G. & Flenner, E. Scaling of the non-phononic spectrum of two-dimensional glasses. *J. Chem. Phys.* **158**, 126101 (2023).
29. Mocanu, F. C. et al. Microscopic observation of two-level systems in a metallic glass model. *J. Chem. Phys.* **158**, 014501 (2023).
30. Shiraishi, K., Hara, Y. & Mizuno, H. Low-frequency vibrational states in ideal glasses with random pinning. *Phys. Rev. E* **106**, 054611 (2022).
31. Rainone, C., Bouchbinder, E. & Lerner, E. Pinching a glass reveals key properties of its soft spots. *Proc. Natl. Acad. Sci. USA* **117**, 5228–5234 (2020).
32. Malandro, D. & Lacks, D. J. Relationships of shear-induced changes in the potential energy landscape to the mechanical properties of ductile glasses. *J. Chem. Phys.* **110**, 4593–4601 (1999).
33. Maloney, C., & Lemai^tr, A. Universal breakdown of elasticity at the onset of material failure. *Phys. Rev. Lett.* **93**, 195501 (2004).
34. Manning, M. L. & Liu, A. J. Vibrational modes identify soft spots in a sheared disordered packing. *Phys. Rev. Lett.* **107**, 108302 (2011).
35. Tong, H. & Xu, N. Order parameter for structural heterogeneity in disordered solids. *Phys. Rev. E.* **90**, 010401(R) (2014).
36. Xu, N., Liu, A. J. & Nagel, S. R. Instabilities of jammed packings of frictionless spheres under load. *Phys. Rev. Lett.* **119**, 215502 (2017).
37. Xu, D., Zhang, S., Liu, A. J., Nagel, S. R. & Xu, N. Discontinuous instabilities in disordered solids. *Proc. Natl. Acad. Sci. USA* **120**, e2304974120 (2023).
38. Wang, L. & Xu, N. Probing the glass transition from structural and vibrational properties of zero-temperature glasses. *Phys. Rev. Lett.* **112**, 055701 (2014).
39. Wang, L. & Xu, N. Non-monotonic pressure dependence of the dynamics of soft glass-formers at high compressions. *Soft Matter* **8**, 11831–11838 (2012).
40. Widmer-Cooper, A., Perry, H., Harrowell, P. & Reichman, D. R. Irreversible reorganization in a supercooled liquid originates from localized soft modes. *Nat. Phys.* **4**, 711–715 (2008).

41. Brito, C. & Wyart, M. Heterogeneous dynamics, marginal stability and soft modes in hard sphere glasses. *J. Stat. Mech. Theor. Exp.* **2007**, L08003 (2007).
42. Chen, K. et al. Measurement of correlations between low-frequency vibrational modes and particle rearrangements in quasi-two-dimensional colloidal glasses. *Phys. Rev. Lett.* **107**, 108301 (2011).
43. Liu, A. J. & Nagel, S. R. The jamming transition and the marginally jammed solid. *Annu. Rev. Condens. Matter Phys.* **1**, 347–369 (2010).
44. van Hecke, M. Jamming of soft particles: geometry, mechanics, scaling and isostaticity. *J. Phys. Condens. Matter* **22**, 033101 (2010).
45. Das, P. & Procaccia, I. Universal density of low-frequency states in amorphous solids at finite temperatures. *Phys. Rev. Lett.* **126**, 085502 (2021).
46. Bouchbinder, E., Lerner, E., Rainone, C., Urbani, P. & Zamponi, F. Low-frequency vibrational spectrum of mean-field disordered systems. *Phys. Rev. B* **103**, 174202 (2021).
47. Folena, G. & Urbani, P. Marginal stability of soft anharmonic mean field spin glasses. *J. Stat. Mech. Theor. Exp.* **2022**, 053301 (2022).
48. Shimada, M., Mizuno, H. & Ikeda, A. Vibrational spectrum derived from local mechanical response in disordered solids. *Soft Matter* **16**, 7279–7288 (2020).
49. Shimada, M. & De Giuli, E. Random quench predicts universal properties of amorphous solids. *SciPost Phys.* **12**, 090 (2022).
50. Buchenau, U. et al. Interaction of soft modes and sound waves in glasses. *Phys. Rev. B* **46**, 2798 (1992).
51. Ramos, M. A., Gil, L., Bringer, A. & Buchenau, U. The density of tunneling and vibrational states of glasses within the soft-potential model. *Phys. Status Solidi A* **135**, 477 (1993).
52. Gurarie, V. & Chalker, J. T. Bosonic excitations in random media. *Phys. Rev. B* **68**, 134207 (2003).
53. Gurevich, V. L., Parshin, D. A. & Schober, H. R. Anharmonicity, vibrational instability, and the boson peak in glasses. *Phys. Rev. B* **67**, 094203 (2003).
54. Schirmacher, W. Some comments on fluctuating-elasticity and local oscillator models for anomalous vibrational excitations in glasses. *J. Non-Cryst. Solids* **357**, 518 (2011).
55. Marruzzo, A., Schirmacher, W., Fratalocchi, A. & Ruocco, G. Heterogeneous shear elasticity of glasses: the origin of the boson peak. *Sci. Rep.* **3**, 1–7 (2013).
56. Sastry, S., Debenedetti, P. G. & Stillinger, F. H. Signatures of distinct dynamical regimes in the energy landscape of a glass-forming liquid. *Nature* **393**, 554–557 (1998).
57. Dagois-Bohy, S., Tighe, B. P., Simon, J., Henkes, S. & van Hecke, M. Soft-sphere packings at finite pressure but unstable to shear. *Phys. Rev. Lett.* **109**, 095703 (2012).
58. Goodrich, C. P. et al. Jamming in finite systems: Stability, anisotropy, fluctuations, and scaling. *Phys. Rev. E* **90**, 022138 (2014).
59. Ninarello, A., Berthier, L. & Coslovich, D. Models and algorithms for the next generation of glass transition studies. *Phys. Rev. X* **7**, 021039 (2017).
60. Berthier, L., Charbonneau, P., Ninarello, A., Ozawa, M. & Yaida, S. Zero-temperature glass transition in two dimensions. *Nat. Commun.* **10**, 1508 (2019).
61. Khomenko, D., Scalliet, C., Berthier, L., Reichman, D. R. & Zamponi, F. Depletion of two-level systems in ultrastable computer-generated glasses. *Phys. Rev. Lett.* **124**, 225901 (2020).
62. Yeh, W.-T., Ozawa, M., Miyazaki, K., Kawasaki, T. & Berthier, L. Glass stability changes the nature of yielding under oscillatory shear. *Phys. Rev. Lett.* **124**, 225502 (2020).
63. Degiuli, E., Laversanne-Finot, A., Düring, G., Lerner, E. & Wyart, M. Effects of coordination and pressure on sound attenuation, boson peak and elasticity in amorphous solids. *Soft Matter* **10**, 5628–5644 (2014).
64. Franz, S., Parisi, G., Urbani, P. & Zamponi, F. Universal spectrum of normal modes in low-temperature glasses. *Proc. Natl. Acad. Sci. USA* **112**, 14539–14544 (2015).
65. Pérez-Castañeda, T., Rodríguez-Tinoco, C., Rodríguez-Viejo, J. & Ramos, M. A. Suppression of tunneling two-level systems in ultrastable glasses of indomethacin. *Proc. Natl. Acad. Sci. USA* **111**, 11275–11280 (2014).
66. Ramos, M. A., Pérez-Castañeda, T., Jiménez-Riobóo, R. J., Rodríguez-Tinoco, C. & Rodríguez-Viejo, J. Do tunneling states and boson peak persist or disappear in extremely stabilized glasses? *J. Low Temp. Phys.* **41**, 412–418 (2015).
67. Pogna, E. A. A., Chumakov, A. I., Ferrante, C., Ramos, M. A. & Scopigno, T. Tracking the connection between disorder and energy landscape in glasses using geologically hyperaged amber. *J. Phys. Chem. Lett.* **10**, 427–432 (2019).
68. Yu, Y. et al. The ω^3 scaling of the vibrational density of states in quasi-2D nanoconfined solids. *Nat. Commun.* **13**, 3649 (2022).
69. Tong, H., Hu, H., Tan, P., Xu, N. & Tanaka, H. Revealing inherent structural characteristics of jammed particulate packings. *Phys. Rev. Lett.* **122**, 215502 (2019).
70. Zhang, S. et al. Local and global measures of the shear moduli of jammed disk packings. *Phys. Rev. E* **107**, 054903 (2023).
71. Bitzek, E., Koskinen, P., Gähler, F., Moseler, M. & Gumbsch, P. Structural relaxation made simple. *Phys. Rev. Lett.* **97**, 170201 (2006).
72. https://software.intel.com/en-us/mkl/.

Acknowledgements

We thank A.J. Liu for useful discussions. D.X., S.Z., H.T., and N.X. acknowledge the support from the National Natural Science Foundation of China (Grant Nos. 12334009, 12074355, and 12274392). L.W. acknowledges the support from the National Natural Science Foundation of China (Grant Nos. 12374202 and 12004001), Anhui Projects (Grant Nos. 2022AH020009, S020218016, and Z010118169), and Hefei City (Grant No. Z020132009). We also thank the Supercomputing Center of the University of Science and Technology of China, the Hefei Advanced Computing Center, and the Beijing Super Cloud Computing Center for the computer time.

Author contributions

N.X. designed the project. D.X. and S.Z. performed the simulations. D.X., S.Z., H.T., L.W. and N.X. analyzed the data and wrote the paper. L.W. and N.X. supervised the project.

Competing interests

The authors declare no competing interests.

Additional information

Supplementary information The online version contains supplementary material available at https://doi.org/10.1038/s41467-024-45671-8.

Correspondence and requests for materials should be addressed to Lijin Wang or Ning Xu.

Peer review information *Nature Communications* thanks Jie Zhang and the other anonymous reviewer(s) for their contribution to the peer review of this work. A peer review file is available.